ЖЭТФ, 2009, том 135, вып. 2, стр. 242–252

EXPERIMENTAL INVESTIGATION OF MUON-CATALYZED $t+t$ FUSION

L. N. Bogdanova[a], **V. R. Bom**[b], **A. M. Demin**[c], **D. L. Demin**[d], **C. W. E. van Eijk**[b], **S. V. Filchagin**[c], **V. V. Filchenkov**[d], **N. N. Grafov**[d*], **S. K. Grishechkin**[c], **K. I. Gritsaj**[d], **A. D. Konin**[d], **A. V. Kuryakin**[c], **S. V. Medved'**[d], **R. K. Musyaev**[c], **A. I. Rudenko**[d], **D. P. Tumkin**[c], **Yu. I. Vinogradov**[c], **A. A. Yukhimchuk**[c], **S. A. Yukhimchuk**[d], **V. G. Zinov**[d], **S. V. Zlatoustovskii**[c]

[a] *State Scientific Center of Russian Federation, Institute of Theoretical and Experimental Physics 117218, Moscow, Russia*

[b] *Delft University of Technology 2629 JB Delft, the Netherlands*

[c] *Russian Federal Nuclear Center, All-Russian Research Institute of Experimental Physics 607200, Sarov, Nizhny Novgorod region, Russia*

[d] *Joint Institute for Nuclear Research, Dzhelepov Laboratory of Nuclear Problems 141980, Dubna, Moscow region, Russia*

Received July 15, 2008

The muon-catalyzed fusion (μCF) process in tritium was studied by the μCF collaboration on the muon beam of the JINR Phasotron. The measurements were carried out with a liquid tritium target at the temperature 22 K and density approximately 1.25 of the liquid hydrogen density (LHD). Parameters of the μCF cycle were determined: the $tt\mu$ muonic molecule formation rate $\lambda_{tt\mu} = 2.84(0.32)\,\mu\text{s}^{-1}$, the tt fusion reaction rate $\lambda_f = 15.6(2.0)\,\mu\text{s}^{-1}$, and the probability of muon sticking to helium $\omega_{tt} = 13.9(1.5)\,\%$. The results agree with those obtained earlier by other groups, but better accuracy was achieved due to our unique experimental method.

PACS: 36.10.Ee, 36.10.-k, 25.30.Mr

1. INTRODUCTION

Investigation of the muon-catalyzed fusion (μCF) tt reaction

$$t + t \longrightarrow {}^4\text{He} + n + n + 11.3\,\text{MeV} \qquad (1)$$

is of great interest for the complete understanding of the μCF processes in a mixture of hydrogen isotopes and for the study of the nuclear reaction mechanism.

The simplified scheme of μCF kinetics in tritium is shown in Fig. 1. In pure tritium, the stopped muons form μt atoms with a high rate λ_a (about $10^{10}\,\mu\text{s}^{-1}$). In their collisions with T_2 molecules, muonic molecules $tt\mu$ are produced nonresonantly with the rate $\lambda_{tt\mu}$ in the rotational–vibrational state $J = v = 1$. Fusion from this state competes with muonic molecule deex-

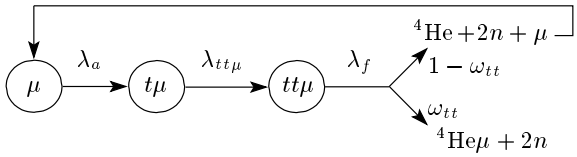

Fig. 1. Diagram of μCF kinetics in tritium

*E-mail: grafov@nusun.jinr.ru

citation via Auger transitions to lower levels and with the muon decay. The main deexcitation channel is the $E0$ Auger transitions to the $(J,v)=(1,0)$ state, its rate being $\lambda_{11\to10}\approx 2\cdot10^8$ s^{-1} [1]. The deexcitation via the electric dipole transition, which changes the total angular momentum J, is characterized by a significantly smaller rate, since in molecules with identical nuclei, such a transition necessarily changes the total spin of nuclei and is suppressed. This rate is estimated as $\lambda_{\Delta J=1}\lesssim 10^4$ s^{-1} [1], which is smaller than the muon decay rate $\lambda_0=0.455\,\mu$s^{-1}, and the role of such transitions is negligible in cascade deexcitation. Thus, the fusion reaction in the $tt\mu$-molecule occurs from the states $J=1$, $v=1,0$ with a rate λ_f. After fusion, the muon is either released with the probability $1-\omega_{tt}$ and can catalyze a new fusion cycle, or is stuck to the helium nucleus with the probability ω_{tt}.

The μCF tt-cycle is characterized by the $tt\mu$ cycling rate

$$\lambda_C=\frac{\lambda_f\lambda_{tt\mu}}{\lambda_f+\lambda_{tt\mu}}. \tag{2}$$

The $tt\mu$-molecule formation rate $\lambda_{tt\mu}$, the fusion reaction rate λ_f, and the coefficient ω_{tt} of muon sticking to helium are the main parameters of the μCF tt cycle.

A unique possibility of studying low-energy (about 0.1 keV) p-wave tt fusion (1) is given by the muon catalysis [2]. Until presently, the p-wave contribution to the tt-fusion cross section has not been determined in collisional experiments at low energies, which are complicated by the three-body final state analysis [3]. In μCF experiments, the p-wave reaction constant can be deduced from the experimentally determined μCF fusion rate λ_f. In addition, the spectra of fusion neutrons, complemented with data on the muon sticking probability, can allow distinguishing the reaction mechanism. The value of the muon sticking coefficient ω_{tt} is sensitive to the energy spectrum of α-particles, which somehow reflects particle correlations in the three-body final state. According to calculations in [4], ω_{tt} is respectively equal to 18 %, 5 %, or 10 % for αn, nn, or no correlations (phase space).

Observation of αn or nn correlations in the p-wave tt fusion can shed light on the possible cluster structure of the 1^--levels in the lightest neutron-rich nucleus ^{6}He.

However, experimental investigations of the μCF tt process also face the problem of a continuous neutron energy spectrum of an unknown character. It is difficult to definitely calculate the neutron detection efficiency ϵ_n for using it in the data analysis.

The way to obtain the μCF parameters without knowing ϵ_n was suggested in [5], where expressions for the total yield η_{all} (the average of cycles per muon), the yield η_1 of the first cycle, and η_k for the kth cycle were obtained for the first time. They are

$$\eta_{all}=\frac{\lambda_{tt\mu}}{\lambda_0+\lambda_{tt\mu}\omega_{tt}},\quad \eta_1=\frac{\lambda_{tt\mu}}{\lambda_0+\lambda_{tt\mu}},$$

$$\eta_k={\eta_1}^k(1-\omega_{tt})^{k-1}.$$

With the theoretical values of the tt μCF parameters in [4, 6, 7], we obtain $\eta_{all}\approx 3$ and $\eta_1\approx 0.8$. The measured yields are $\eta\epsilon_c$, where ϵ_c is the detection efficiency per cycle (detection of at least one neutron from the tt reaction).

It follows from the analysis in [5] that the value of ω_{tt} can be directly determined from the ratio of measured yields of the first detected neutrons (η_1) and the second ones (η_2):

$$1-\omega_{tt}=\frac{\eta_2}{\eta_1^2}. \tag{3}$$

This additional condition allows determining the $t+t$ μCF parameters without knowing ϵ_n.

But this method is difficult because it involves large statistics, since it requires accumulation of the order of 10^4 second neutrons. This becomes a problem when the value of ϵ_c is limited.

So far, two experiments were performed by the PSI and RIKEN–RAL groups to determine the main parameters of the μCF tt-cycle. The results of these experiments do not completely agree with each other.

In the experiment performed at the muon channel of the PSI meson facility [8], the efficiency was $\epsilon_n\approx 1$ % and the authors could accumulate a few thousand second neutrons and, consequently, obtained an accuracy about 20–30 % for the μCF parameters. The other experiment was carried out by the RIKEN–RAL group [9] at the pulsed beam of the RAL accelerator. The authors could determine the slope of the "slow" component (see below) of the neutron time spectrum. To extract λ_C, they made a rough determination of the neutron yield Y_n in the tt reaction with a 20 % accuracy.

The main feature of our experiment is the use of a unique neutron detection system consisting of two high-efficiency neutron detectors placed symmetrically around the target. The high value $\epsilon_n\approx 30$ % allows high statistics, which is important for the accuracy of the μCF parameters, and, besides, allows an independent study of the reaction mechanism by measurement of the neutron energy spectrum. The geometry of the installation provides the opportunity to reveal the faint $n-n$ correlation in the final state of reaction (1).

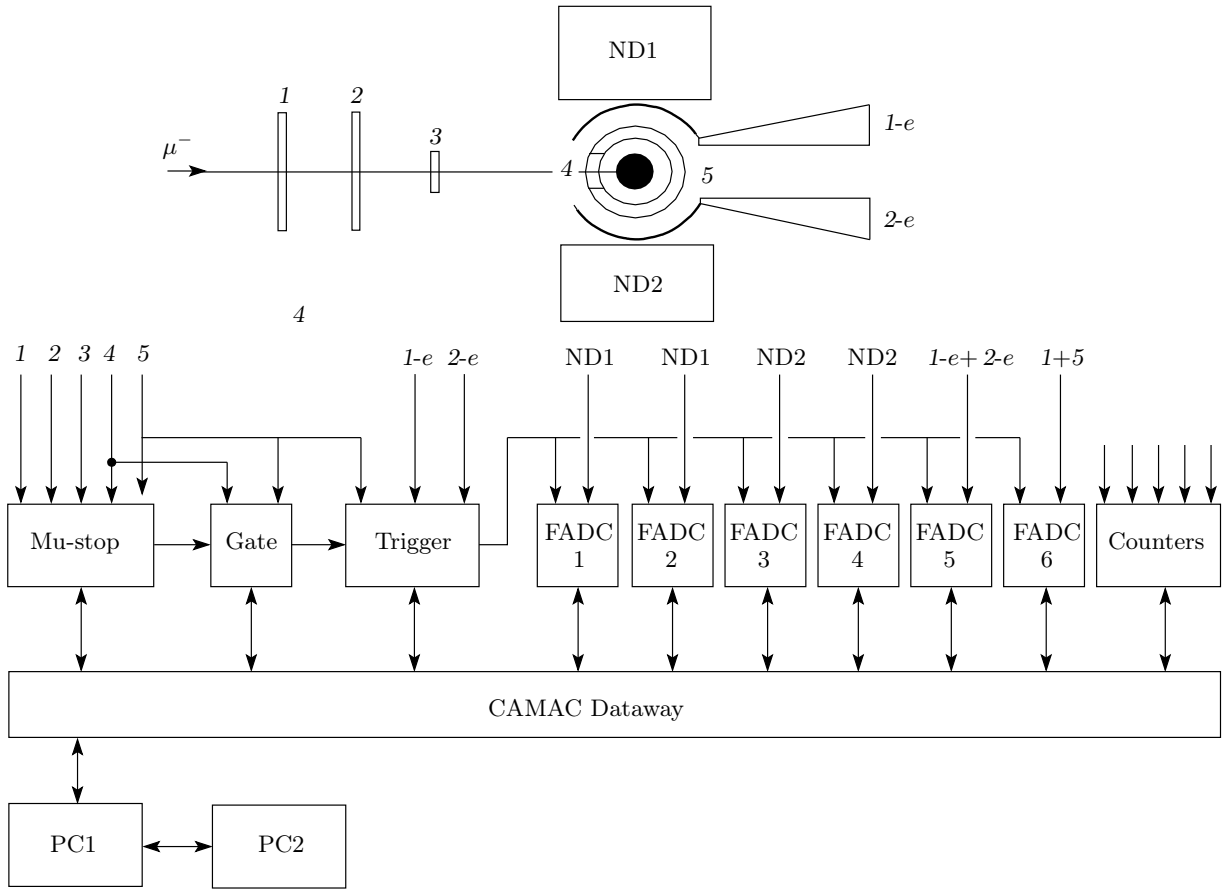

Fig. 2. Experimental lay-out

2. EXPERIMENT

The experimental setup is analogous to our previous experiments on μCF [10–12] with some minor changes. The experiment was performed at the installation "Triton" mounted on the muon channel [13] of the JINR Phasotron. The experimental setup is schematically shown in Fig. 2. The target (depicted in Fig. 2 as a black circle) was surrounded by a set of detectors.

2.1. Detectors and electronics

Scintillation counters *1–3* detected incoming muons. Cylinder-shaped proportional counters *4* and *5* (analogous to those described in [14]) served to select muon stops in the target (signal $1{\cdot}2{\cdot}3{\cdot}4{\cdot}\bar{5}$) and to detect electrons from muon decay. Specially designed cylinder-shaped scintillation counters *1-e* and *2-e* were used to detect μ-decay electrons in coincidence with counter *5* (signals $5{\cdot}1\text{-}e$ and $5{\cdot}2\text{-}e$ were considered μ-decay electrons). The full absorption neutron spectrometer (FANS) [15] consisting of two large detectors (ND1 and ND2), each of the volume 12.5 l , was the basis of the detection system. Its aim was to detect neutrons from reaction (1).

The timing sequences of the signals from the detectors ("oscillograms") were registered by six flash ADCs (2048 samples of 8 bits at 100 Mc/s), depicted in Fig. 2 as FADC 1–6, and were recorded on the PCs. An example of the "oscillograms" for one muon measured in the test run is shown in Fig. 3.

FADCs 1 and 3 were used to read the shortened (30 ns) signals from the NDs. With FADCs 2 and 4, the neutron–gamma ($n-\gamma$) separation of the ND signals was realized to discriminate the background. Each ND signal was transformed into a double signal whose parts corresponded to the integral of the "fast" (50 ns) and "slow" (200 ns) components of the ND light pulse. Thus, the signal analysis time was $\Delta t = 250$ ns. The comparison of the "fast" and the "slow" charges allowed realizing the $n-\gamma$ separation (see Fig. 4). The γ-quantum discrimination efficiency was better than 10^{-3} for energies larger than 100 keV.

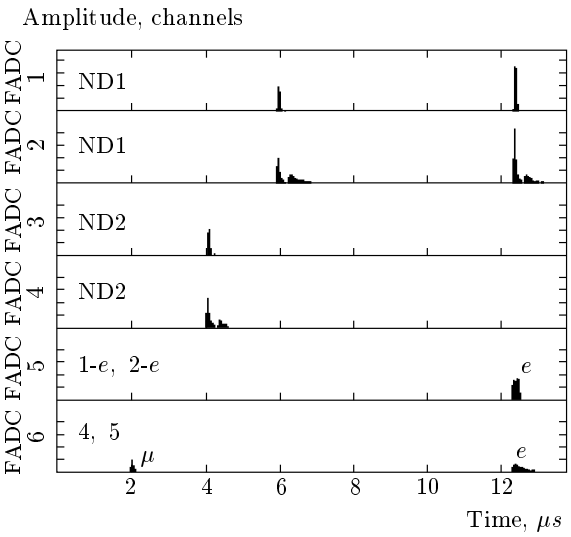

Fig. 3. Example of the "oscillograms" for one muon measured in the test run

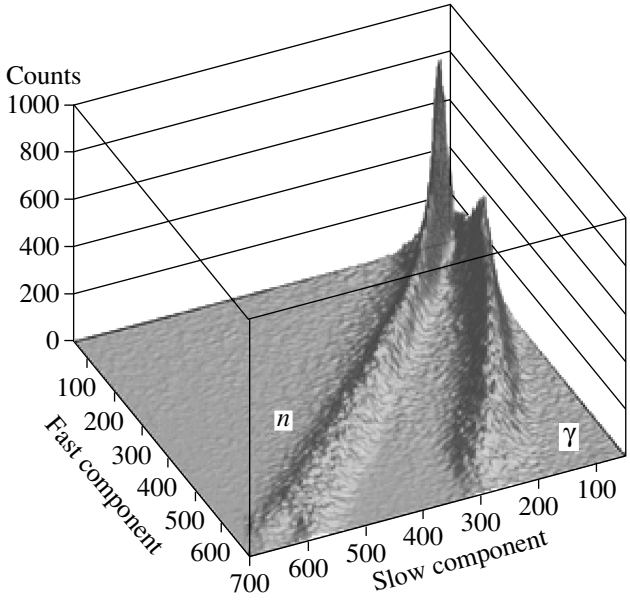

Fig. 4. Three-dimensional plot characterizing the ratio of the amplitudes of fast and slow components of the ND signal

Finally, FADCs 5 and 6 registered the signals of the muon stop and the μ-decay electron.

The trigger [16] allowed recording only those events that were connected with the electron detection. During each run, the data were also monitored on-line.

2.2. Target and gas handling system

In the experiment, a new liquid-tritium target (LTT) with the working volume 10 cm^3 [17] was used. The LTT was filled with liquid tritium (amounting to about 3.6 cm^3 — about 10 kCi — the ecological limit for our installation), and kept at the temperature about 22 K with the tritium pressure about 1 atm. To fill the LTT and maintain the required temperature regime, a cryogenic refrigerator was used. A preparation system [18] provided *in-situ* purification of the tritium gas. The chromatography method was used to monitor the isotopic and molecular composition of the tritium gas [19].

2.3. Temperature, pressure, and density control

The temperature of liquid tritium was determined by measuring the vapor pressure with tensometric gauges that were accurate to 0.5 %. The temperature was thus determined to be 22.5 K with the accuracy 0.1 K.

The nuclear density of liquid tritium was determined using cryogenic data on hydrogen isotopes [20]. We obtained the value 1.25 LHD (±1 %).

2.4. Liquid tritium purity and ^{3}He accumulation

The muon transfer from $t\mu$ atoms to possible impurities influences the measured value of the sticking probability. To reduce this influence for accurate determination of ω_{tt}, the condition

$$\lambda_Z C_Z \ll \omega_{tt}\lambda_{tt\mu} \tag{4}$$

must be satisfied, where C_Z is the fraction of the impurities and λ_Z is the rate of muon transfer to them. It was necessary to distinguish three sorts of impurities: those with $Z > 2$, helium, and hydrogen isotope admixtures.

Impurities with $Z > 2$. The impurities with $Z > 2$ consisted predominantly of carbon, oxygen, and nitrogen. The gas preparation system based on palladium filters [18] provided target fillings with the purification level of $C_Z < 10^{-7}$ volume parts. The rate of muon transfer from the $t\mu$ atom to the admixtures of nuclei with $Z > 2$ is $\lambda_Z \sim 10^{11}$ s^{-1} [21]. Therefore, condition (4) was satisfied.

^{3}He admixture. The tritium preparation system provided the initial ^{3}He concentration in tritium $C_{\mathrm{He}} \sim 10^{-7}$ before pouring it into a target. However,

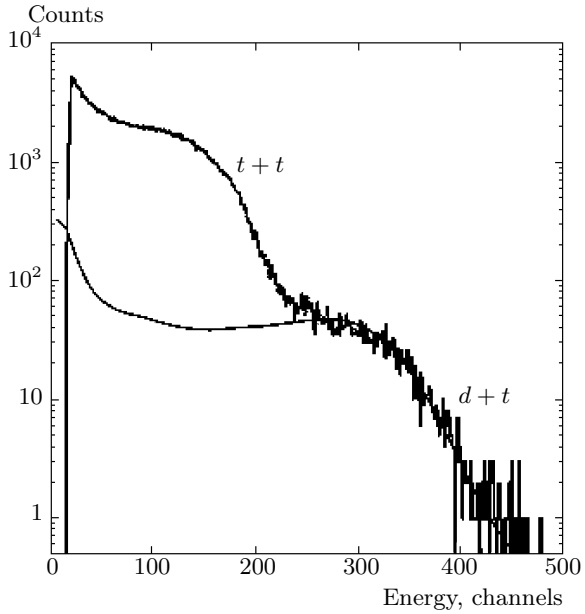

Fig. 5. ND charge spectra measured in the present experiment. The lower line corresponds to the contribution of dt neutrons. The edge for 14 MeV dt neutrons corresponds to about 400 ch

due to the tritium β-decay, ^{3}He was accumulated in the target in accordance with the relation

$$C_{\mathrm{He}}(\tau) = C_t[1 - \exp(-\lambda_{trit}\tau)],$$

where $\lambda_{trit} = 1.8 \cdot 10^{-9}$ s^{-1} is the tritium decay rate. Hence, the process of muon transfer from the $t\mu$ atom to ^{3}He (with the rate $\lambda_{^3\mathrm{He}} \approx 2 \cdot 10^8$ s^{-1} [22]) could significantly influence the rate of muon loss.

In the experiment in [23], it was shown that ^{3}He in liquid tritium diffuses and goes out to the vapor (gas phase). Therefore, there were no problems about the liquid tritium purity with respect to the elements with $Z > 1$ in our experiment. This was confirmed by the coincidence between the observed muon disappearance rate and the muon decay rate (see Sec. 3.1 below).

Deuterium and protium admixture in tritium. In this experiment, we used tritium with some initial admixture of other hydrogen isotopes. We clearly observed the presence of deuterium admixture by the "tail" from 14 MeV neutrons from the reaction

$$dt\mu \to {}^4\mathrm{He}\,(3.5\,\mathrm{MeV}) + n\,(14.1\,\mathrm{MeV}) + \mu \qquad (5)$$

in the measured charge spectrum of fusion neutrons (see Fig. 5).

The chromatographic method [19], which was used to check the level of hydrogen isotope admixture in tritium, showed a presence of less than 1 % of deuterium and protium.

3. DATA ANALYSIS

The first step in the analysis of the registered events was the separation of neutrons, γ-quanta, and μ-decay electrons. Then, for each exposure, we built and analyzed the distributions of time and charge (deposited energy in a neutron detector) of fusion neutrons. The number of μ-decay electrons necessary for normalizing the neutron yield was obtained from the analysis of the electron time distribution.

3.1. Electron time spectra

Time spectra of electrons from muons that stopped and decayed in the target are distorted by the background originating mainly from decay of muons stopping in the target walls. In the run with an empty target, we measured the time spectra of background electrons and obtained the shape of the distribution $B_{empty}(t)$. For the working exposures with a tritium-filled target, we fitted the electron time spectra taking the background shape into account:

$$N_e^{total}(t) = kB_{empty}(t) + A_e \exp(-\lambda_e t) + F,$$

where λ_e is the muon disappearance rate and F is an accidental background. In this fit, the values k, A_e, λ_e, and F were the variables.

The fitted time distribution of decay electrons for the tritium-filled target is shown in Fig. 6. The observed muon disappearance rate $\lambda_e = 0.456(2)\,\mu\mathrm{s}^{-1}$ found by the fit is in a good agreement with the known value for the free muon decay rate $\lambda_0 = 0.455\,\mu\mathrm{s}^{-1}$. As a result, the number of electrons from muon decay in tritium was obtained:

$$N_e = \frac{A_e}{\lambda_e \Delta\tau} = 972000 \pm 2900,$$

where $\Delta\tau = 20$ ns is the channel bin width. The error of N_e was about 0.3 %. It was determined from the uncertainty in fitting the electron time spectra from the filled (0.2 %) and the empty (0.2 %) target and was mainly defined by the total statistics.

3.2. Analysis of the neutron data

We analyzed the neutron time distributions to obtain the μCF parameters. Only the first, second, and third detected neutrons were selected for analysis. Two analysis methods, with and without $n - \gamma$ separation, were applied.

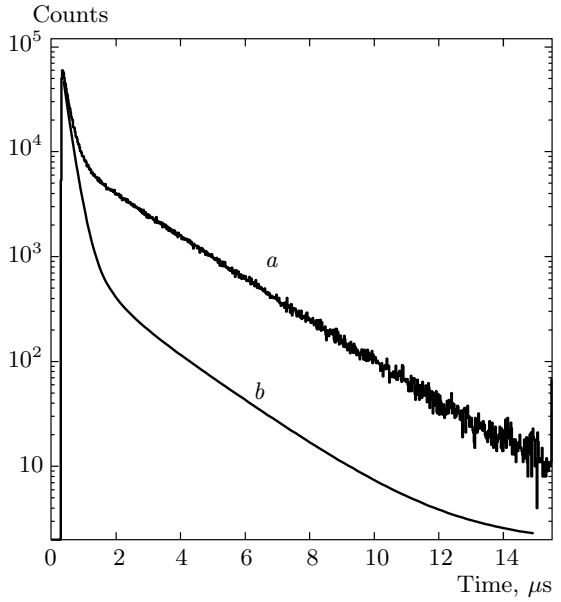

Fig. 6. Electron time distribution. The line a is the optimum fit for the filled target, the line b corresponds to electrons from the empty target

3.2.1. Selection of events

1. In the analysis with the $n-\gamma$ separation, the events were selected by the shape of the ND signal. To exclude pile-up in the time interval $\Delta t = 250$ ns required for the signal analysis, the detected neutrons were specifically selected.

a) The first neutron was accepted if the time between the first and the second neutron t_{1-2} was larger than Δt. If $t_{1-2} < \Delta t$, we rejected all neutrons caused by this muon.

b) The second neutron was accepted if the time between the second and the third neutron t_{2-3} was larger than Δt and $t_{1-2} > \Delta t$. If $t_{1-2} > \Delta t$ and $t_{2-3} < \Delta t$, we accepted only the first neutron from all neutrons caused by this muon.

The presence of pile-up was under direct control due to fast signals on FADCs 1 and 3. In the present experiment, we found the probability of pile-up within the interval Δt to be

$$\delta \approx 5\text{–}6\,\%\,.$$

2. The method with the $n-\gamma$ separation required that the analysis be made separately for each ND because of their different parameters. The large neutron detection efficiency of our detectors can lead to simultaneous registration of two neutrons from the reaction: two neutrons were registered either a) in the same detector (one signal) or b) in different NDs (two signals). In determining the μCF parameters, we should deal with the number of μCF cycles, not with the number of neutrons. Therefore, in case b), we were forced to take only one neutron in an arbitrarily chosen ND and to reject the other neutron.

3. To reduce the background, the time selection criterion

$$t_n + 0.3\,\mu\text{s} < t_e < t_n + 10\,\mu\text{s}$$

was used [24], where t_n and t_e are neutron and electron detection times measured from the moment of a muon stop in the target. The lower bound discriminated the background due to muon stops in the target wall, and the upper bound decreased the accidental background caused by false electrons.

3.2.2. Analytic expressions used for the analysis of neutron time spectra

The kinetics of μCF processes in tritium was considered first in [5] and then, in more detail, in [24], where Monte Carlo test calculations were performed, in addition to the analytic consideration. The time distribution of the first detected neutrons (cycles) has the form of the difference of two exponentials:

$$\frac{dN_1}{dt} \equiv f_1(t) = A[\exp(-\gamma_1 t) - \exp(-\gamma_2 t)]. \qquad (6)$$

The amplitude A and the slopes γ_1 and γ_2 were determined from the fit of the experimental spectrum. The $tt\mu$ cycling rate λ_C and other cycle parameters can then be evaluated.

The slopes γ_1 and γ_2 were expressed through the cycle parameters as

$$2\gamma_1 = \lambda_f + \lambda_{tt\mu} + 2\lambda_0 - \\ - [(\lambda_f + \lambda_{tt\mu})^2 - 4\alpha\lambda_f\lambda_{tt\mu})]^{1/2}, \qquad (7)$$

$$2\gamma_2 = \lambda_f + \lambda_{tt\mu} + 2\lambda_0 + \\ + [(\lambda_f + \lambda_{tt\mu})^2 - 4\alpha\lambda_f\lambda_{tt\mu})]^{1/2}, \qquad (8)$$

$$\alpha \equiv \epsilon_c + \omega_{tt}(1-\epsilon_c).$$

The time distribution of the second detected neutrons was

$$\frac{dN_2}{dt} \equiv f_2(t) = A^2 \left[(\exp(-\gamma_1 t) + \exp(-\gamma_2 t))\, t + \right. \\ \left. + \frac{2}{\gamma_2 - \gamma_1} (\exp(-\gamma_1 t) - \exp(-\gamma_2 t)) \right]. \qquad (9)$$

It was shown in [24] that the dead time interval (Δt) does not change the shape of the time distribution for

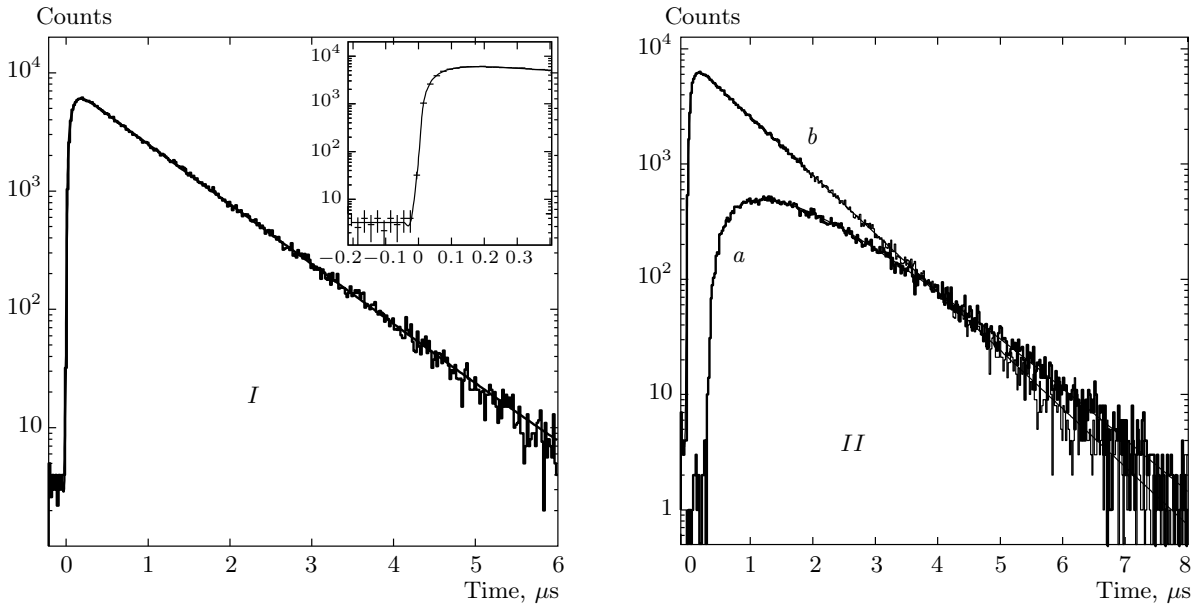

Fig. 7. Time distributions of the first and second detected neutrons with $n-\gamma$ separation. The solid lines present the optimum fits. I — time distribution of neutrons from dt reactions. II — time distributions of the first (b) and second (a) neutrons from tt reactions

the first neutrons. However, the neutron yields were changed. This led to a modification of expression (3) used for direct determination of ω_{tt}. The first neutron yield is

$$\eta_1' = \eta_1(1-(1-\omega_{tt})\delta). \tag{10}$$

The loss in the first neutron yield η_1 connected with the dead time selection is 5–6 %.

For the second neutrons, the corresponding yield is

$$\eta_2' = \eta_2\left(1-\frac{\delta}{\eta_1}\right)(1-(1-\omega_{tt})\delta)\,. \tag{11}$$

In this case, the loss was more significant and constituted about 20 %. From Eqs. (3), (10), and (11), we obtained the relation connecting the measured yields η_1' , η_2', δ, and ω_{tt}:

$$\frac{\eta_2'}{(\eta_1')^2} = (1-\omega_{tt})\frac{1-\delta/\eta_1}{1-(1-\omega_{tt})\delta}. \tag{12}$$

3.2.3. Analysis with $n-\gamma$ separation

Being a means of background suppression, the $n-\gamma$ analysis was a source of statistics loss. Besides the necessity to introduce a dead time, we had to remove the events with registration of 4.43 MeV γ's produced in the inelastic threshold process $n(^{12}\mathrm{C},\gamma)n'$ (only for neutrons with high energy, more than 5 MeV). They distorted the ND signal and had to be rejected. It is important to note that both factors lead not to ambiguities in the determination of μCF parameters but only to a decrease in the total detection efficiency by about 30 %.

The measured time distributions of the first and second detected neutrons are shown in Fig. 7.

The distribution of the first neutrons was analyzed using Eq. (6). The parameters of this expression (the amplitude A and the exponent slopes $\gamma_{1,2}$) were functions of λ_f and $\lambda_{tt\mu}$ (formulas (2), (7), and (8)). In addition, we measured the numbers of first, N_1, and second, N_2, detected neutrons and obtained the respective yields η_1 and η_2:

$$\eta_1 = \frac{N_1}{N_e}, \quad \eta_2 = \frac{N_2}{N_e}, \quad \eta_1', \quad \eta_2'.$$

These yields were used for the determination of ω_{tt} in accordance with expressions (10), (11), and (12). Using these yields and the values A and $\gamma_{1,2}$ obtained from the fit of the measured time distribution, we reconstructed the tt cycle parameters, λ_f, $\lambda_{tt\mu}$, and ω_{tt}, as well as the neutron detection efficiency ϵ_n.

Influence of *dt* neutrons. A deuterium impurity of about 0.5–1 % contained in the tritium resulted in an admixture of DT molecules (about 0.02) and also of D_2 molecules (about 0.0001) in liquid T_2. The rates

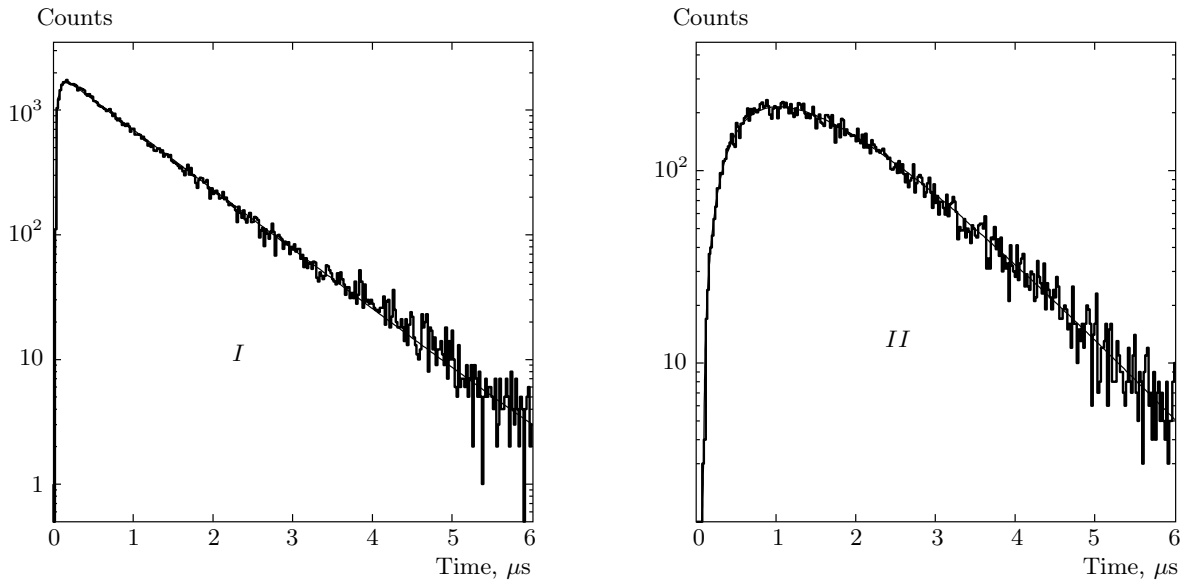

Fig. 8. Time distributions of the second neutrons with respect to the first ones (I) and of the third neutrons relative to the second ones (II). The curves are the respective fitting functions (6) and (9) with the optimum parameters

of $dt\mu$ muonic molecule formation on these molecules measured at the temperature 22 K were given by [12]

$$\lambda_{dt\,\mu-\mathrm{DT}} \approx 10\,\mu\mathrm{s}^{-1}, \quad \lambda_{dt\,\mu-\mathrm{DD}} \approx 800\,\mu\mathrm{s}^{-1}.$$

The formation of $dt\,\mu$, molecules becomes essential at such rates and the presence of 14 MeV neutrons from the dt reaction

$$dt\mu \to n + {}^4\mathrm{He} + \mu$$

is noticeable in all measured spectra. The amplitude A and the slopes λ_{fast} and λ_{slow} of the first neutron time spectrum, as well as the neutron yields η_1 and η_2 were distorted. The necessary corrections of distortions caused by the dt neutrons were taken into account in the analysis.

In our work on muon catalyzed dt fusion [12], the calculated neutron spectrum was in good agreement with the measured one. We could use the known shape of the 14 MeV neutron spectrum from the dt reaction. Analyzing the neutron charge spectrum shown in Fig. 5, we estimated the fraction of dt-neutrons in all distributions. We obtained this contribution as approximately (3.67±0.27) %. This allowed accurate subtraction of the dt neutron spectrum from the time distribution of the first neutrons. We thus avoided any distortion in the final results of the μCF tt parameters (mainly in λ_f).

The time distribution of first neutrons for the dt "tail" did not show a "fast" component. This was natural for dt neutrons, because the dt fusion rate was high (about 10^{12} s^{-1}). The slope of the dt neutron time spectrum exponent was practically the same as the "slow" component for the whole neutron time distribution. Therefore, dt neutrons did not change the "slow" component λ_{slow} of the tt neutron time spectrum.

Because the nuclear density for D_2 and DT molecules was less than $0.01\,LHD$, the epithermal "spike" in the dt spectrum, appearing when $t\mu$ atoms pass through the resonances of muonic molecule formation rates [25], should manifest itself. We observed this spike in the present measurement, as in our previous [26] and PSI [27] experiments.

3.2.4. Analysis without $n-\gamma$ separation

The procedure of $n-\gamma$ separation allowed reliable discrimination of the background but significantly complicated the data interpretation and led to some systematic ambiguities. It was desirable to find an independent analysis method that would allow checking the obtained data and verifying the results.

Analyzing the γ-background revealed that it was predominantly concentrated just in the time region of a muon stop. We therefore decided to also make an analysis without $n-\gamma$ separation. Treating the time of the first neutron as the time of a muon stop in the target, the second neutron as the first and the third

Table 1. μCF parameters of the tt cycle determined in the present experiment by two analysis methods

Value	with $n-\gamma$	without $n-\gamma$	combined
$\lambda_{tt\mu}$, $10^6 s^{-1}$	2.96 ± 0.32	2.56 ± 0.33	2.84 ± 0.32
λ_f, $10^6\, s^{-1}$	15.2 ± 2.0	15.9 ± 2.1	15.6 ± 2.0
ω_{tt}, %	13.2 ± 1.5	14.6 ± 1.7	13.9 ± 1.5

one as the second, we plotted the distributions of time difference between second–first and third–first neutrons without $n-\gamma$ separation. For these distributions, we obtained the numbers of neutrons N_{2-1} and N_{3-1}. The background turned out to be small enough in this case (only a few percent) and could easily be determined and subtracted. The correspondingly measured distributions are shown in Fig. 8.

This method was rather simple and suitable but led to a noticeable decrease in the neutron statistics. For the method with $n-\gamma$ separation, the losses in statistics were relatively small (about 30 %). For the second method, the losses appeared to be larger:

$$1 - \eta_1 \approx 0.6\text{–}0.7.$$

To significantly (twice) increase the statistics, we performed a combined analysis for both ND counters considering them as one detector. So we succeeded in obtaining approximately equal statistical power for both analysis methods. The advantage of the combined method is that it allows detecting two neutrons simultaneously, and hence correcting the $n-\gamma$ analysis.

The analysis procedure and consideration of the dt background were analogous to the previous approach. Naturally, expression (3) instead of (10)–(12) was used for the determination of ω_{tt}. The time distributions of the first and second neutrons are shown in Fig. 8 together with best-fit functions (6) and (9).

3.2.5. Results of the main tt μCF parameters

The main μCF parameters (λ_f, $\lambda_{tt\mu}$, and ω_{tt}) obtained by two methods are presented in Table 1. The errors include both statistical and systematical uncertainties. Statistical errors in λ_f and $\lambda_{tt\mu}$ were determined by the total number of events and the character of the fitting functions. The statistical error in ω_{tt} was combined from the uncertainties of the components (N_e, N_1^2, and N_2) and of the ratio η_2/η_1^2 in Eq. (2).

The main sources of systematic errors were:

a) an uncertainty of 1.3 % in the value of tritium density was included in the total error for $\lambda_{tt\mu}$;

b) an uncertainty of 2.1 % due to nonexact knowledge of the deuterium impurity was included in the error for ω_{tt}.

It is seen from Table 1 that both methods give the same result within 15 %. This allows assigning the combined values as final results.

4. DISCUSSION AND CONCLUSION

The experimental data on the main tt μCF parameters (the $tt\mu$-molecule formation rate $\lambda_{tt\mu}$, the fusion rate λ_f, and the sticking probability ω_{tt}) are summarized in Table 2 in comparison with the theoretical predictions.

Results of all experiments show general agreement with the theoretical predictions. In our experiment, the accuracy of the $tt\mu$-molecule formation rate was improved by a factor of two, and the value of $\lambda_{tt\mu}$ is close to the theoretical one. Our fusion rate λ_f agrees with the PSI result [8] and is somewhat larger than the estimate in [28], based on the in-flight data [3]. Another theoretical estimate [29] is a few times larger than the observed one.

The fusion rate λ_f can be expressed in terms of the reaction constant and the so-called fusion integral ρ_{1v}:

$$\lambda_f = K_{odd}\rho_{1v} \tag{13}$$

(the Deser factorization relation [30]). The reaction constant K_{odd} is spin-dependent, and the subscript "odd" means that only triplet spin states of two tritons contribute in the p-wave, due to the antisymmetry of the wave function for identical fermions. The fusion integral

$$\rho_{1v} = \frac{1}{2}\int d^3r\, |\nabla_R \Psi_{1v}(\mathbf{r}, \mathbf{R})|_{R=0}$$

involves the normalized $tt\mu$ Coulomb wave function (R is the internuclear distance, r is the muon coordinate, and the factor of $1/2$ is required because of the wave

Table 2. Parameters of the tt μCF

Parameter	Source	Ref	Value
$\lambda_{tt\mu}$, 10^6 s^{-1}	PSI experiment	[8]	1.8 ± 0.6
	RIKEN–RAL experiment	[9]	2.4 ± 0.6
	Present experiment		2.84 ± 0.32
	Theory	[6]	2.96
	Theory	[7]	2.64
λ_f, 10^6 s^{-1}	PSI experiment	[8]	15 ± 2
	RIKEN–RAL experiment	[9]	no
	Present experiment		15.6 ± 2.0
	Theory	[28]	13
ω_{tt}, %	PSI experiment	[8]	14 ± 3
	RIKEN–RAL experiment	[9]	8.7 ± 1.9
	Present experiment		13.9 ± 1.5
	Theory	[28]	14

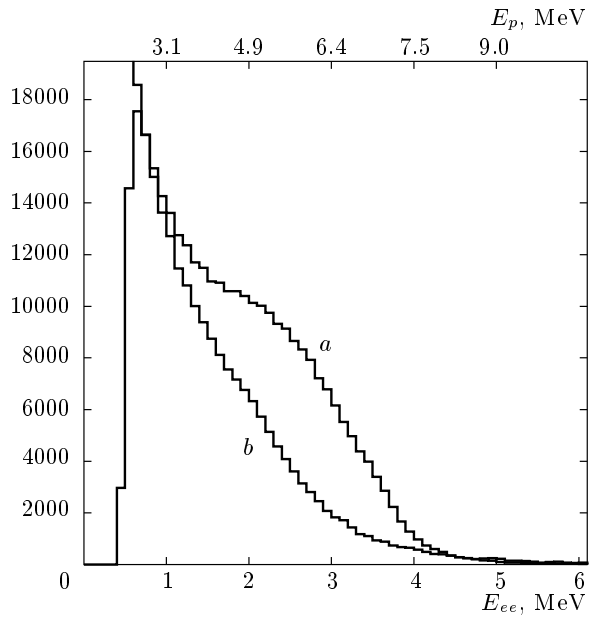

Fig. 9. The neutron energy spectrum measured in this experiment (a) and the calculated neutron energy distribution for pure phase space (b)

function symmetrization). Further, K_{odd} is associated with the spin-dependent cross section via the relation

$$K_{odd} = \lim_{v \to 0} \frac{1}{2} \frac{\sigma_{odd} v C_1^{-2} (vM)^{-2}}{9},$$

where v and M are the relative velocity and the reduced mass of nuclei,

$$C_1^2 = \frac{2\pi\eta(1+\eta^2)}{9(e^{2\pi\eta}-1)},$$

is the p-wave Gamow factor with $\eta = \alpha c/v$ being the Sommerfeld parameter, and $1/2$ is the symmetrization factor of the continuum wave function. Finally, $\sigma_{odd} = (4/3)\sigma_p$, with σ_p being the p-wave cross section for unpolarized particles, where $3/4$ of two triton spin states are odd (triplet), and $K_p = (3/4)K_{odd}$.

Taking the value of ρ_{1v} from [28], we find the p-wave tt-reaction constant as $K_p = 4.3 \cdot 10^{23}$ fm$^5 \cdot$ s^{-1}. A similar value for the dd reaction, obtained from the muon catalysis experiment and from the R-matrix analysis of the dd in-flight fusion data, is $K_p = 10^{25}$ fm$^5 \cdot$ s^{-1} [31].

Our value of the sticking probability ω_{tt} agrees with the PSI result. Twice improved accuracy favors the theoretical value obtained under the assumption of an $\alpha - n$ correlation in the final state of reaction (1). Our value of the cycling rate $\lambda_C = 2.4\,\mu$s^{-1} agrees with the one obtained in [9].

In both experimental works [8, 9], the evidence for $\alpha - n$ correlation was obtained by comparison of the measured recoil proton spectrum of the neutron detector with the one simulated assuming the absence of any final-state correlations. This is supported by the shape of the neutron spectrum obtained in our measurement (Fig. 9). The neutron energy spectrum highlights the features of the reaction mechanism: An $n - n$ correlation would result in a concentration of the events in the region $E_{n1} = E_{n2} = 3.8$ MeV (E_{n1} and E_{n2} are neutron energies); for $\alpha - n$ correlation, the events are grouped near $E_{n1} \approx 9.3$ MeV and $E_{n2} \approx 0.5$ MeV (in a simplified consideration) [2]. A more detailed analysis of the $t+t$ reaction mechanism is in progress. Besides, it would be desirable to make more precise calculations of λ_f.

The measurements of the μCF tt reaction were for the first time performed with the use of a unique method (FANS, FADC). Conditions of high efficiency for neutron registration allowed obtaining the main reaction parameters with higher accuracy compared to earlier experiments.

The authors are grateful to L. I. Ponomarev for stimulating discussions and to C. Petitjean for valuable comments. The work was supported by the Ministry of Atomic Energy of RF (Contract № 6.25.19.19.99.969), by the Ministry of Science and Technology of RF (state contract № 103-7(00)-II), and the RFBR (№ 08-02-16351).

REFERENCES

1. Ya. B. Zeldovich and S. S. Gershtein, Usp. Fiz. Nauk **71**, 581 (1960).
2. L. N. Bogdanova and V. V. Filchenkov, Hyp. Int. **138**, 321 (2001).
3. V. I. Serov, S. N. Abramovich, and L. A. Morkin, Sov. Phys. Atomnaya Energia **42**, 59 (1977); H. M. Agnew et al., Phys. Rev. **84**, 862 (1952).
4. S. S. Gershtein et al., Zh. Eksp. Teor. Fiz. **80**, 1690 (1981) [Sov. Phys. JETP **53**, 872 (1981)].
5. V. V. Filchenkov, L. N. Somov, and V. G. Zinov, Nucl. Instr. Meth. **228**, 174 (1984); Preprint JINR, P15-82-566, Dubna (1982).
6. L. I. Ponomarev and M. P. Faifman, Zh. Eksp. Teor. Fiz. **71**, 1689 (1976) [Sov. Phys. JETP **44**, 886 (1976)].
7. M. P. Faifman, Muon Cat. Fusion **4**, 341 (1989).
8. W. H. Breunlich et al., Muon Cat. Fusion **1**, 121 (1987).
9. T. Matsuzaki et al., Hyp. Int. **118**, 229 (1999); T. Matsuzaki et al., Hyp. Int. **138**, 295 (2001); T. Matsuzaki et al., Phys. Lett. B **557**, 176 (2003).
10. Yu. P. Averin et al., Hyp. Int. **118**, 111 (1998).
11. V. R. Bom et al., Hyp. Int. **138**, 313 (2001).
12. V. R. Bom et al., Zh. Eksp. Teor. Fiz. **127**, 752 (2005) [JETP **100**, 663 (2005)].
13. A. V. Demianov et al., JINR Communication P9-93-374, Dubna (1993).
14. A. D. Konin, JINR Communication P13-82-634, Dubna (1982).
15. V. P. Dzhelepov et al., Nucl. Instr. Meth. A **269**, 634 (1988); V. V. Filchenkov, A. D. Konin, and V. G. Zinov, Nucl. Instr. Meth. A **245**, 490 (1986); V. A. Baranov et al., Nucl. Instr. Meth. A **374**, 335 (1996); V. G. Zinov et al., JINR Communication P13-91-182, Dubna (1991).
16. V. G. Zinov et al., Prib. Techn. Exp. **3**, 38 (1998).
17. A. A. Yukhimchuk et al., Fusion Sci. Tech. **48**, 294 (2005).
18. A. A. Yukhimchuk et al., Hyp. Int. **119**, 341 (1998).
19. A. A. Yukhimchuk et al., Preprint VNIIEF 83-2002, Sarov (2002).
20. M. P. Malkov et al., *Guide to Physico-Technical Base of Cryogenic*, Energoatomizdat, Moscow (1973).
21. L. Schellenberg, Muon Cat. Fusion **5/6**, 73 (1990/91); Hyp. Int. **82**, 513 (1993).
22. B. Gartner et al., Hyp. Int. **119**, 103 (1999).
23. N. Kawamura et al., Hyp. Int. **118**, 213 (1999); N. Kawamura et al., Phys. Lett. B **465**, 74 (1999).
24. D. L. Demin et al., JINR Communication E15-2003-199, Dubna (2003).
25. A. Adamczak et al., At. Nucl. Data Tables **62**, 255 (1996); JINR Preprint E4-95-488, Dubna (1995).
26. V. V. Filchenkov et al., Hyp. Int. **163**, 143 (2005).
27. W. H. Breunlich et al., Phys. Rev. Lett. **53**, 1137 (1984); W. H. Breunlich et al., Muon Cat. Fusion **1**, 67 (1987); M. Jeitler et al., Phys. Rev. A **51**, 2881 (1995).
28. L. N. Bogdanova, Muon Cat. Fusion **3**, 359 (1988).
29. E. Hiyama and M. Kamimura, RIKEN Rev. **20**, 34 (1999).
30. S. Deser et al., Phys. Rev. **96**, 774 (1954).
31. G. M. Hale, Muon Cat. Fusion **5/6**, 227 (1990).